

Using SuZIE arcminute-scale CMB anisotropy data to probe open and flat- Λ CDM cosmogonies

K. Ganga^{1,2}, Bharat Ratra³, S.E. Church¹, Naoshi Sugiyama⁴, P.A.R. Ade⁵,
W.L. Holzzapfel^{1,6}, A.E. Lange¹, and P.D. Mauskopf^{1,7}

ABSTRACT

We use arcminute-scale data from the Sunyaev-Zel'dovich Infrared Experiment to set limits on anisotropies in the cosmic microwave background radiation in open and spatially-flat- Λ cold dark matter cosmogonies. There are no $2\text{-}\sigma$ detections for the models tested. The upper limits obtained are consistent with the amplitude of anisotropy detected by the *COBE*/DMR experiment.

Subject headings: cosmic microwave background—cosmology: observations—large-scale structure of the universe

¹Division of Physics, Mathematics and Astronomy, Mail Stop: 59-33, California Institute of Technology, Pasadena, CA 91125.

²Current address: IPAC, California Institute of Technology, MS 100-22, Pasadena, CA 91125

³Center for Theoretical Physics, Massachusetts Institute of Technology, Cambridge, MA 02139. Current address: Department of Physics, Kansas State University, Manhattan, KS 66506.

⁴Department of Physics, Kyoto University, Kitashirakawa-Oiwakecho, Sakyo-ku, Kyoto 606, Japan.

⁵Department of Physics, Queen Mary and Westfield College, Mile End Road, London, E1 4NS, UK.

⁶Current address: Laboratory for Astrophysics and Space Research, Enrico Fermi Institute, University of Chicago, 5641 S. Ingleside Ave., Chicago, IL 60637.

⁷Current address: Department of Physics and Astronomy, University of Massachusetts at Amherst, Amherst, MA 01003-0120.

1. Introduction

With the detection of anisotropy in the cosmic microwave background (CMB) by the *COBE*/DMR experiment (Smoot et al. 1992; Wright et al. 1992; Bennett et al. 1996) and a host of other detections on angular scales greater than $\sim 10'$ (Ganga et al. 1994; Hancock et al. 1996; Piccirillo et al. 1997; Netterfield et al. 1997; Gundersen et al. 1995; Tucker et al. 1997; Platt et al. 1996; Masi et al. 1996; Tanaka et al. 1996; Inman et al. 1996; Griffin et al. 1997; Scott et al. 1996), CMB anisotropy measurements have become a powerful tool for testing models of cosmic structure formation. At smaller angular scales, however, the detection of anisotropies has proven more difficult (Griffin et al. 1997; Myers et al. 1993; Subrahmanyan et al. 1993). Moreover, calculation of theoretical CMB anisotropies at these angular scales is difficult and has only recently been done accurately. Thus, the detection of arcminute scale anisotropies and their classification is one of the significant hurdles to be overcome in the characterization of the CMB.

In this paper we use arcminute-scale CMB anisotropy data from the Sunyaev-Zel'dovich Infrared Experiment (SuZIE), an experiment designed to measure the Sunyaev-Zel'dovich (SZ) effect in distant clusters of galaxies. These data were taken as part of a program to characterize the instrument for SZ observations, but can be used to set interesting limits on the power spectrum of CMB anisotropies. Theoretical predictions for primary CMB anisotropy spectra are used in conjunction with these data to set limits on the normalization of cosmic structure formation models in low-density open and spatially-flat (with a cosmological constant Λ) cold dark matter (CDM) universes.

2. Data

SuZIE was originally conceived and constructed to make millimeter-wave observations of both the thermal and kinetic SZ effects in clusters of galaxies from the Caltech Submillimeter Observatory on Mauna Kea (Holzapfel et al. 1997a; Wilbanks et al. 1994). It employs a 2×3 array of bolometers cooled to 300 mK, with beam widths of approximately $1.7'$ (FWHM) and beam throws of $\pm 2.3'$ in right ascension (see insets of Figure 1; also Figure 2 of Church et al. 1997). The instrument is described fully by Holzapfel et al. (1997b).

Each pair of detectors in a single row is electronically differenced in an AC bridge, with the output of each bridge phase-synchronously demodulated to produce a DC signal proportional to the difference in power absorbed by the two detectors (Rieke et al. 1989; Wilbanks et al. 1990; Glezer, Lange, & Wilbanks 1992). In terms of atmospheric rejection, this is equivalent to a square wave chop between the two detectors at infinite frequency.

Observations were made at 140 GHz ($\sim 11\%$ bandpass) and were performed by fixing the telescope and using the rotation of the Earth to make the sky ‘drift’ (in right ascension) through the array’s view. This eliminates spurious signals arising from mechanical chopping or motion of the telescope.

The output from the AC bridge, after calibration, gives the difference in temperature between two spots on the sky,

$$\Delta_{ij} = T_i - T_j, \quad (1)$$

where T_i and T_j are the CMB temperature at the two spots on the sky. The focal plane has two rows of three pixels. The rows are separated by $2.0'$ in declination, with the three pixels in each row separated by $2.3'$ in right ascension. The data used here are the differences between the two outermost pixels in each row, detectors 3 and 1 in row 1 and detectors 6 and 4 in row 2, which are separated by $4.6'$ (Figure 1; also see Figure 2 of Church et al. 1997).

Two $36'$ regions of the sky were observed, one centered at R.A. $10^{\text{h}} 21^{\text{m}} 49.00^{\text{s}}$ and Dec. $4^\circ 4' 23.00''$ (Region 1) and the other at R.A. $16^{\text{h}} 30^{\text{m}} 17.00^{\text{s}}$ and Dec. $5^\circ 56' 0.00''$ (Region 2; epoch 1950). The instrument is Nyquist sampled at 5 Hz. The data have an offset and linear drift removed, and are coadded and binned into $45''$ bins. The data are shown in Figure 1 and the zero-lag window function associated with one row of pixels, W_l , is shown in Figure 2. The uncertainty in the gaussian beam widths, estimated at 5%, translate to errors in limits on models primarily through the uncertainty introduced into the calibration. The beam width uncertainties are ignored otherwise (Ganga et al. 1997). The calibration, obtained from scans of Uranus, is known to 8%. The data reduction and calibration are described more fully in Church et al. (1997).

3. Models

The CMB fractional temperature perturbation, $\delta T/T$, can be decomposed into a sum over spherical harmonics according to

$$\frac{\delta T}{T}(\theta, \phi) = \sum_{l=2}^{\infty} \sum_{m=-l}^l a_{lm} Y_{lm}(\theta, \phi). \quad (2)$$

In this scheme, a convenient characterization of the CMB anisotropy is its angular power spectrum, C_l , defined in terms of the ensemble average

$$\langle a_{lm} a_{l'm'}^* \rangle = C_l \delta_{ll'} \delta_{mm'}. \quad (3)$$

Prior to the construction of semi-realistic cosmogonies, it was conventional to use a gaussian parameterization for the CMB anisotropy spectrum. The fiducial CDM (fCDM) model, an Einstein-de Sitter cosmological model with gaussian, adiabatic, scale-invariant energy-density perturbations (Harrison 1970; Peebles & Yu 1970; Zel’dovich 1972), focussed attention on what has now come to be known as the flat angular spectrum (Peebles 1982),

$$C_l = \frac{6C_2}{l(l+1)} = \frac{24\pi(Q/T_0)^2}{5l(l+1)}. \quad (4)$$

In this context, Q , sometimes referred to as $Q_{\text{rms-PS}}$, is the *implied* quadrupole amplitude of the CMB anisotropy spectrum and T_0 is the present CMB temperature. Q should not be confused with the actual amplitude of the quadrupole moment of the CMB anisotropy, to which SuZIE is not sensitive. This spectrum is shown as the straight, solid line in Figure 2.

The flat spectrum is simply a large-scale approximation of the fCDM spectrum. On smaller scales, the pressure of the photon-baryon fluid causes the spectrum to deviate from this approximation. The fCDM spectrum, with standard recombination, $h = 0.5$, and baryonic-mass density parameter $\Omega_B = 0.0125h^{-2}$, is shown as the dotted line in Figure 2. Here, the Hubble parameter $H_0 = 100h \text{ km s}^{-1} \text{ Mpc}^{-1}$. Although still of some historical interest, the fCDM model, which has a clustered-mass density parameter $\Omega_0 = 1$, is now known to be an inadequate representation of the observed universe.

Low-density CDM cosmogonies, with flat spatial sections and a cosmological constant or with open spatial sections and no Λ , are consistent with a large fraction of present observations. For flat- Λ models, see Stompor, Górski, & Banday (1995), Ostriker & Steinhardt (1995), Ratra et al. (1997), Liddle et al. (1996), and Ganga, Ratra, & Sugiyama (1996), and for open models see Kamionkowski et al. (1994), Ratra et al. (1997), Ganga et al. (1996), and Górski et al. (1996). Since the low-density Λ -CDM models are assumed to have flat spatial sections, the simplest power spectrum for gaussian, adiabatic, energy-density perturbations is the scale-invariant one. The simplest spectrum for these perturbations consistent with open spatial sections is that which is generated by quantum-mechanical fluctuations during an early epoch of inflation in an open model (Ratra & Peebles 1994, 1995; Bucher, Goldhaber, & Turok 1995; Yamamoto, Sasaki, & Tanaka 1995). The values of the parameters Ω_0 , h and Ω_B which characterize the spectra in the low-density CDM models used here are chosen to be roughly consistent with present observational estimates of Ω_0 , h , the age of the universe, and the constraints on Ω_B that follow from the observed light element abundances in the standard nucleosynthesis model (Ratra et al. 1997; see Table 1 for parameter values). A standard recombination open model spectrum and a standard recombination flat- Λ model spectrum are shown in Figure 2.

The general procedure for the computation of CMB anisotropy spectra is discussed

by Sugiyama (1995). Since SuZIE is sensitive to sub-arcminute-scale anisotropies, we have computed the open model spectra to $l = 7500$, where photon diffusion strongly suppresses the power. Photon diffusion cuts off power on larger scales in the fiducial and flat- Λ CDM models, so we have only computed the spectra in these models up to $l = 3500$.

4. Analysis

As a starting point for our analysis, we note that Church et al. (1997) have shown that the reduced χ^2 's for each of the data sets used here are less than one. This gives us a good indication that the data does not show a detection; i.e., it is consistent with experimental noise. As shown below, this is indeed the case. To set numerical limits on various cosmological models, however, and in order to compare the results obtained for different models, we use a more refined technique.

A primary goal of CMB anisotropy observations is to measure the angular spectrum of the fluctuations. Given the width of the SuZIE window function, it is not possible to extract a value for each multipole moment to which the experiment is sensitive. Rather, one can hope, at best, to determine a few observational numbers with reasonable accuracy. It is therefore necessary to simplify the problem by assuming a model for the spectrum over the range of l to which the experiment is sensitive. Typically, one assumes a functional form for the shape of the spectrum as a function of l , with the overall normalization allowed to be a free parameter. The shape of the spectrum can also depend on other free parameters. One then compares this family of spectra to the data and determines the value of the normalization and other parameters which best reproduce the data.

For the purpose of the following discussion we assume that the SuZIE sky signal is purely CMB without any offset or gradient, which would have been removed during data reduction. Following Bond et al. (1991) to account for the baseline removal, the likelihood, at the nominal calibration, corresponding to a given spectrum is

$$L \propto \frac{1}{\sqrt{\det(\mathbf{f}^T \mathbf{M}^{-1} \mathbf{f}) \det(\mathbf{M})}} e^{-\chi^2/2}, \quad (5)$$

where,

$$\chi^2 = \Delta^T (\mathbf{M}^{-1} - \mathbf{M}^{-1} \mathbf{f} (\mathbf{f}^T \mathbf{M}^{-1} \mathbf{f})^{-1} \mathbf{f}^T \mathbf{M}^{-1T}) \Delta. \quad (6)$$

Here, Δ is the vector of temperature differences and \mathbf{M} is the correlation matrix of the data in the context of the model considered. The correlation matrix, \mathbf{M} , is the sum of correlations arising from experimental noise, \mathbf{S} , and those from correlations intrinsic to the CMB, \mathbf{C} . That is, $\mathbf{M} = \mathbf{C} + \mathbf{S}$. In the case of SuZIE, the noise correlation matrix

is approximately diagonal, with the diagonal elements simply equal to the variance of the corresponding measurement. This is true so long as atmospheric correlations and other correlations induced in the process of reducing the data can be ignored (Church et al. 1997). \mathbf{C} is calculated according to

$$C_{ij} = \frac{1}{4\pi} \sum_l (2l+1) C_l W_{ijl}, \quad (7)$$

where

$$W_{ijl} = \frac{16\pi}{2l+1} B_{il} B_{jl} \sum_{m=1}^l \left[\frac{\sin(m\Phi_b/2)}{m\Phi_b/2} \right]^2 [1 - \cos(m\Phi_0)] \hat{P}_{lm}(\theta_i) \hat{P}_{lm}(\theta_j) \cos[m(\phi_i - \phi_j)]. \quad (8)$$

Here $B_{il} = \exp[-l(l+1)\sigma_i^2/2]$ is the Legendre transform of the i^{th} beam, assumed to be gaussian, Φ_b is the extent of a single data bin in right ascension, $0.75' \times \cos \delta$ in this case, and Φ_0 is the azimuthal separation of the two points differenced in a single sample, $4.6'$. θ is the declination of the pixel above or below the *center* of the array ($\pm 1'$), and \hat{P}_{lm} is defined by

$$Y_{lm}(\theta, \phi) = \hat{P}_{lm}(\theta) \cdot e^{im\phi}. \quad (9)$$

See Bond (1996) and White & Srednicki (1995) for general discussions of CMB window functions. In eqs. (5) and (6), \mathbf{f} is the array of functions that have been fit out of the data (in this case an offset and gradient from each channel; it is thus an 96×4 matrix for each region).

With this prescription, all models yield the same likelihood at $Q = 0 \mu\text{K}$ (i.e., nothing but noise), providing a convenient way to normalize across models.

Following Ganga et al. (1997), we account for calibration uncertainty by taking

$$\mathcal{L} = \frac{1}{\sqrt{2\pi} \sigma_C Q} \times \int_0^\infty dQ' e^{-(Q'-Q)^2/[2(\sigma_C Q)^2]} L(Q'), \quad (10)$$

where σ_C is the fractional uncertainty in the calibration, 0.08. This is conservative since it assumes the calibration uncertainty is completely correlated in all detectors. This is the case if there is an error in the model of the calibration source, but does not apply if the uncertainties are statistical, due to, for example, uncertainty in the beam measurements.

This calibration-uncertainty-corrected likelihood is computed for all the models considered. Assuming a uniform prior in Q gives a posterior probability density distribution equal to the likelihood function.

For the models considered here there are no $2\text{-}\sigma$ anisotropy detections, defined according to the prescription discussed in Ganga et al. (1997; also see Berger 1985). To

quantify the constraints, we quote two different $2\text{-}\sigma$ upper limits for each model and data set considered. The highest posterior density (HPD) prescription provides the smallest possible $2\text{-}\sigma$ upper limit. In this scheme, the upper and lower $2\text{-}\sigma$ limits on Q , Q_u and Q_l , are defined such that

$$\int_{Q_l}^{Q_u} \mathcal{L} \cdot dQ = 0.9545 \times \int_0^\infty \mathcal{L} \cdot dQ, \quad (11)$$

and $Q_u - Q_l$ is *minimized*. Here, Q_l is zero for all models, indicating that there are no detections. The equal tail (ET) prescription gives a larger $2\text{-}\sigma$ upper limit, calculated using

$$\int_0^{Q_u} \mathcal{L} \cdot dQ = 0.9772 \times \int_0^\infty \mathcal{L} \cdot dQ. \quad (12)$$

Finally, we note that expected sky rms can be written as a sum of contributions from different multipoles, $\delta T_{\text{rms}}^2 = \sum_l (\delta T_{\text{rms}}^2)_l$, where

$$(\delta T_{\text{rms}}^2)_l = T_0^2 \frac{(2l+1)}{4\pi} C_l W_l. \quad (13)$$

In Figure 3 we plot this quantity for the four representative spectra shown in Figure 2. This plot indicates that though the SuZIE window function peaks at $l \sim 2400$, with $l_{\text{eff}} \sim 2340$ and $l_{e-0.5} \sim 1330$ and 3670 (as defined by Bond 1996), the SuZIE sensitivity is model dependent. In these models SuZIE is most sensitive to multipoles $l \lesssim 1000$, and is still sensitive down to $l \sim 200$.

5. Results and Discussion

Table 1 lists the $2\text{-}\sigma$ upper limits on Q . Also listed are the limits on the bandtemperature, δT_l , obtained using the upper limits on Q , equation (13), and

$$\delta T_l = \sqrt{\frac{\delta T_{\text{rms}}^2}{\sum_{l=2}^\infty \left[\frac{(l+1/2)W_l}{l(l+1)} \right]}}. \quad (14)$$

Note that δT_l is *not* a function of l (Bond 1996, also see Ganga et al. 1997, eq. [7]). Like δT_{rms} , δT_l should be fairly independent of the model, but unlike δT_{rms} , it can also be compared to results from experiments with different window functions. The degree to which δT_l varies from model to model gives an indication of how good the flat bandpower approximation is.

Figure 4 shows representative likelihood functions for the combined SuZIE data and some of the models considered.

In all cases, the SuZIE 2- σ upper limits on Q are consistent with, and less restrictive than, the detections obtained by the *COBE/DMR* experiment. In general, these limits are lower for the open models than for the flat- Λ models. The 2- σ upper limits on δT_l are much less model dependent than the Q limits. There remains, however, a $\sim 25\%$ difference in δT_l between the two extreme cases, indicating that using the flat bandpower approximation to calculate the expected signal that should be seen by an experiment is not accurate at these angular scales.

Like open CDM cosmogonies, anti-tilted flat- Λ models ($n > 1$) predict more power on arcminute angular scales than do flat- Λ models without tilt ($n = 1$). The SuZIE 2- σ upper limits on Q for models with $\Omega_0 = 0.3$, $h = 0.6$, $\Omega_B h^2 = 0.0175$ and $n = 1.2$ and 1.4 are $18 \mu K$ and $11 \mu K$ (HPD), respectively. These can be compared to the limits for the twenty-first model of Table 1, which has $n = 1$. When these results are combined with the *COBE/DMR* result, it is likely that spectral indices of order 1.5 or larger can be ruled out for this particular cosmogony.

Atmospheric noise is a concern for all ground based CMB anisotropy experiments. Because we have assumed that the experimental noise is gaussian, if it were to be significantly non-gaussian it could change the limits set here. In order to check this, we have examined histograms of the data in each bin and found them sufficiently gaussian. We have also repeated the above analysis including estimates of the correlations induced by the atmosphere (Church et al. 1997). In all cases, these limits are comparable to or less than those quoted above without the atmospheric corrections. Contributions from dust at these angular scales are not expected to be significant (Tegmark & Efstathiou 1996).

Since the telescope is generally stationary while data is taken, SuZIE is mostly immune to problems caused by motion of the instrument. Between scans, however, the telescope slews, raising the possibility of temperature drifts in the instrument at the beginning of a new scan. To check that this is not an issue, we repeated the above analysis excluding the first seven bins in each scan. The results were qualitatively the same as those from the entire data set, with limits a bit less strict, numerically consistent with the loss of data. Church et al. (1997) have done a more sophisticated analysis by correlating the data with the temperature of the SuZIE 300 mK stage and come to the same conclusion.

We have checked that the truncated spectra used here does not affect the results by “filling in” the C_l spectra to $l = 10000$ using the C_l value at the largest computed l value. As one might expect from an inspection of Figure 3, the numbers do not change to the accuracy quoted here.

6. Conclusion

The SuZIE has been used to set limits on primary anisotropies in the CMB at arcminute angular scales. Though there are no detections in this data set, the likelihood functions shown in Figure 4 peak tantalizingly close to the maximum likelihood Q values obtained from the *COBE*/DMR data, lending hope that CMB fluctuations will soon be detected on arcminute scales. Even if they are not, however, increased sensitivity may allow for meaningful limits to be set on cosmological parameters such as Ω_0 or the spectral index of primordial fluctuations.

The next generation version of the SuZIE instrument, SuZIE 1.5, is now operational and has taken data simultaneously in three wavelength bands: 1.1, 1.4, and 2.1 mm (Mauskopf et al. 1997). These three bands correspond to three atmospheric windows near the peak brightness of the CMB and close to the minimum in the confusion expected from astrophysical sources on these angular scales (Fischer & Lange 1993). The new receiver's ability to observe simultaneously in these three bands will allow residual atmospheric noise, which limited the sensitivity of the previous instrument, to be identified by its frequency correlation between channels and then removed.

We thank Thor Wilbanks for contributions to the SuZIE instrument and for help with the observations. This work was supported in part by NASA grant NAGW-4623 and by National Science Foundation grant AST-95-03226. BR was supported in part by National Science Foundation grant EPS-9550487 and matching support from the state of Kansas. NS was supported by Grant-in-aid for Scientific Research No. 8740193 from the Ministry of Education of Japan. The CSO is operated by the California Institute of Technology under funding from the National Science Foundation, contract AST-93-13929.

Table 1: SuZIE Region 1, 2, and Combined 2- σ Upper Limits on Q and δT_l (in μK) for Various Models^a

			Q (HPD) ^b			Q (ET) ^c			δT_l	
Ω_0	h	$\Omega_B h^2$	R. 1	R. 2	R. 1 & 2	R. 1	R. 2	R. 1 & 2	HPD ^b	ET ^c
0.1	0.75	0.0125	37	29	24	42	33	27	40	44
0.2	0.65	0.0175	42	35	28	49	40	31	40	46
0.2	0.70	0.0125	45	38	30	53	44	33	40	46
0.2	0.75	0.0075	50	43	33	58	50	37	40	46
0.3	0.60	0.0175	42	36	27	49	42	31	41	46
0.3	0.65	0.0125	45	40	29	53	46	33	41	46
0.3	0.70	0.0075	51	47	33	60	55	38	41	47
0.4	0.60	0.0175	40	36	26	48	42	30	41	47
0.4	0.65	0.0125	44	41	28	52	48	32	41	47
0.4	0.70	0.0075	50	50	33	60	59	38	42	48
0.5	0.55	0.0175	36	33	23	42	38	26	41	47
0.5	0.60	0.0125	39	38	25	47	44	29	42	48
0.5	0.65	0.0075	46	48	30	56	57	35	43	49
1.0	0.50	0.0125	51	60	35	62	70	41	46	53
0.1	0.90	0.0125	64	72	46	75	82	53	47	55
0.2	0.80	0.0075	66	78	50	77	86	58	50	59
0.2	0.75	0.0125	57	66	40	69	76	46	47	54
0.2	0.70	0.0175	53	57	35	63	67	41	45	52
0.3	0.70	0.0075	61	74	45	73	83	52	50	58
0.3	0.65	0.0125	53	60	36	64	70	41	46	54
0.3	0.60	0.0175	47	51	31	58	60	36	45	52
0.4	0.65	0.0075	59	72	43	71	82	50	50	58
0.4	0.60	0.0125	50	58	34	61	68	39	46	54
0.4	0.55	0.0175	45	48	29	55	57	34	45	52
0.5	0.60	0.0075	51	59	34	62	69	40	46	54
Flat Bandpower			36	29	26	41	32	28	40	44

^aThe first 13 models are open CDM, the 14th is fCDM, the 11 following fCDM are flat- Λ CDM models and, finally, the flat spectrum model is at the bottom. The quoted values of δT_l are determined using the data from both Regions 1 & 2.

^bThe HPD prescription is described in eq. [11].

^cThe EQ prescription is described in eq. [12].

REFERENCES

- Bennett, C.L., et al. 1996, ApJ, 464, L1
- Berger, J.O. 1985, Statistical Decision Theory and Bayesian Analysis (New York: Springer-Verlag)
- Bond, J.R., Efstathiou, G., Lubin, P.M., & Meinhold, P.R. 1991, Phys. Rev. Lett., 66, 2179
- Bond, J.R. 1996, in Cosmology and Large Scale Structure, ed. R. Schaeffer, J. Silk, M. Spiro, & J. Zinn-Justin (Dordrecht: Elsevier Science Publishers), in press
- Bucher, M., Goldhaber, A.S., & Turok, N. 1995, Phys. Rev. D, 52, 3314
- Bunn, E.F. & Sugiyama, N. 1995, ApJ, 446, 49
- Church, S.E., et al. 1997, ApJ, submitted
- Fischer, M.L., & Lange, A.E. 1993, ApJ, 419, 433
- Ganga, K., Page, L., Cheng, E., & Meyer, S. 1994, ApJ, 432, L15
- Ganga, K., Ratra, B., & Sugiyama, N. 1996, ApJ, 461, L61
- Ganga, K., Ratra, B., Gundersen, J.O., & Sugiyama, N. 1997, ApJ, 484, in press
- Glezer, E.N., Lange, A.E., & Wilbanks, T.M. 1992, Applied Optics, 31, 7214
- Górski, K.M., et al. 1994, ApJ, 430, L89
- Górski, K.M., Ratra, B., Sugiyama, N., & Banday, A.J. 1995, ApJ, 444, L65
- Górski, K.M., et al. 1996, MIT preprint MIT-CTP-2548
- Griffin, G.S., et al. 1997, in preparation
- Gundersen, J.O., et al. 1995, ApJ, 443, L57
- Hancock, S., et al. 1996, MNRAS, submitted
- Harrison, E.R. 1970, Phys. Rev. D, 1, 2726
- Holzappel, W.L., et al. 1997a, ApJ, in press
- Holzappel, W.L., et al. 1997b, ApJ, in press
- Inman, C.A., et al. 1996, ApJ, submitted
- Kamionkowski, M., Ratra, B., Spergel, D.N., & Sugiyama, N. 1994, ApJ, 434, L1
- Liddle, A.R., Lyth, D.H., Viana, P.T.P., & White, M. 1996, MNRAS, 282, 281
- Masi, S., et al. 1996, ApJ, 463, L47
- Mauskopf, P.D., et al. 1997, in preparation

- Myers, S.T., Readhead, A.C.S., & Lawrence, C.R. 1993, *ApJ*, 405, 8
- Netterfield, C.B., et al. 1997, *ApJ*, 474, 47
- Ostriker, J.P., & Steinhardt, P.J. 1995, *Nature*, 377, 600
- Peebles, P.J.E. 1982, *ApJ*, 263, L1
- Peebles, P.J.E., & Yu, J.T. 1970, *ApJ*, 162, 815
- Piccirillo, L., et al. 1997, *ApJ*, 475, L77
- Platt, S.R., et al. 1997, *ApJ*, 475, L1
- Ratra, B., & Peebles, P.J.E. 1994, *ApJ*, 432, L5
- Ratra, B., & Peebles, P.J.E. 1995, *Phys. Rev. D*, 52, 1837
- Ratra, B., Sugiyama, N., Banday, A.J., & Górski, K.M. 1997, *ApJ*, 481, in press
- Rieke, F.M., Lange, A.E., Beeman, J.W., & Haller, E.E. 1989, *IEEE Trans. Nucl. Sci.*, 36, 946
- Scott, P.F., et al. 1996, *ApJ*, 461, L1
- Smoot, G.F., et al. 1992, *ApJ*, 396, L1
- Stompor, R., Górski, K.M., & Banday, A.J. 1995, *MNRAS*, 277, 1225
- Subrahmanyam, R., Ekers, R.D., Sinclair, M., & Silk, J. 1993, *MNRAS*, 263, 416
- Sugiyama, N. 1995, *ApJS*, 100, 281
- Tanaka, S.T., et al. 1996, *ApJ*, 468, L81
- Tegmark, M., & Efstathiou, G. 1996, *MNRAS*, 281, 1297
- Tucker, G.S., et al. 1997, *ApJ*, 475, L73
- White, M., & Srednicki, M. 1995, *ApJ*, 443, 6
- Wilbanks, T.M., et al. 1990, *IEEE Trans. Nucl. Sci.*, 37, 556
- Wilbanks, T.M., et al. 1994, *ApJ*, 427, L75
- Wright, E.L., et al. 1992, *ApJ*, 396, L13
- Yamamoto, K., Sasaki, M., & Tanaka, T. 1995, *ApJ*, 455, 412
- Zel'dovich, Ya.B. 1972, *MNRAS*, 160, 1P

Figure Captions

Fig. 1.— Measured temperature differences on the sky as a function of scan position. The upper two panels show data from the two detector rows for Region 1, the lower two panels show data from the two detector rows for Region 2. As stated in the text, each of the four data sets correspond to the differences between two of the six pixels, as represented schematically by the six circles in each plot. Each pixel is separated from its neighbors by $2.3'$ in right ascension and $2'$ in declination. The filled circles indicate the pixels being differenced for each data plot. See Church et al. (1997) for a full description of the data reduction.

Fig. 2.— SuZIE zero-lag window function ($W_l \equiv W_{iil}$ in eq. [8]; scale on right axis) and four primary CMB anisotropy spectra normalized to the DMR two-year data (scale on left axis). The open, flat- Λ and fCDM spectra are computed for $\Omega_B h^2 = 0.0125$. The open CDM, fCDM and flat spectra are normalized to the DMR galactic-frame maps (Górski et al. 1994, 1995; also see Ratra et al. 1997), the flat- Λ spectrum is normalized to the DMR ecliptic-frame maps (Bunn & Sugiyama 1995; also see Ratra et al. 1997), and in all cases the quadrupole moment is excluded from the analysis of the DMR data. Since the DMR four-year data have been completely analyzed for only some of the models considered here, we use the DMR two-year data normalizations, bearing in mind that the four-year data indicates values for Q which are $\sim 10\%$ smaller than those obtained with the two-year data (e.g., Górski et al. 1995, 1996). The flat bandpower $2\text{-}\sigma$ (HPD) upper limit obtained here is placed at the location of the window function peak. See, however, Figure 3.

Fig. 3.— $(\delta T_{\text{rms}}^2)_l$ (eq. [14]), as a function of l for the CMB anisotropy spectra shown in Figure 2. These curves should be compared to the SuZIE window function shown in Figure 2. Note the multiple “sensitivity” peaks for each spectrum, and that the major contributions to the signals arise from multipole values lower than those indicated by considering the window function (Figure 2) alone.

Fig. 4.— Likelihood functions given the combined Regions 1 and 2 SuZIE data, for the four CMB anisotropy angular spectra of Figure 2.

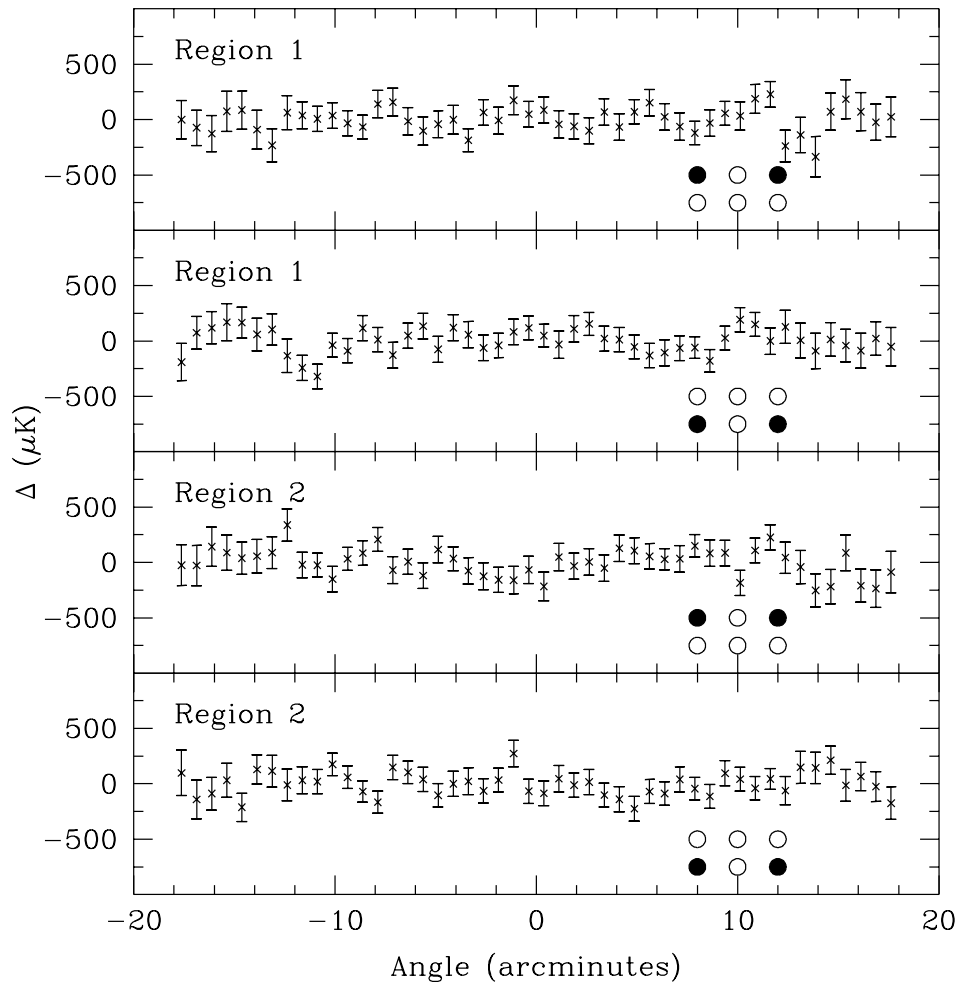


Figure 1

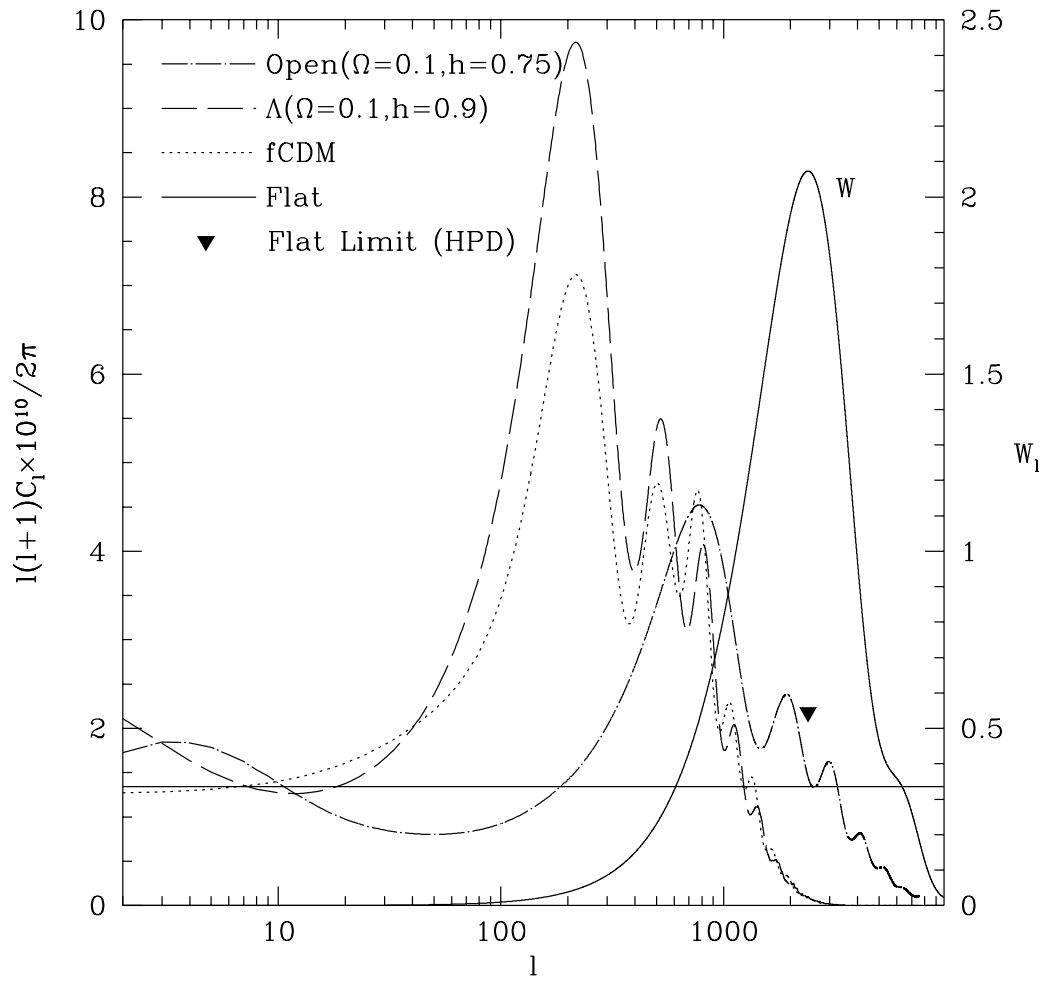


Figure 2

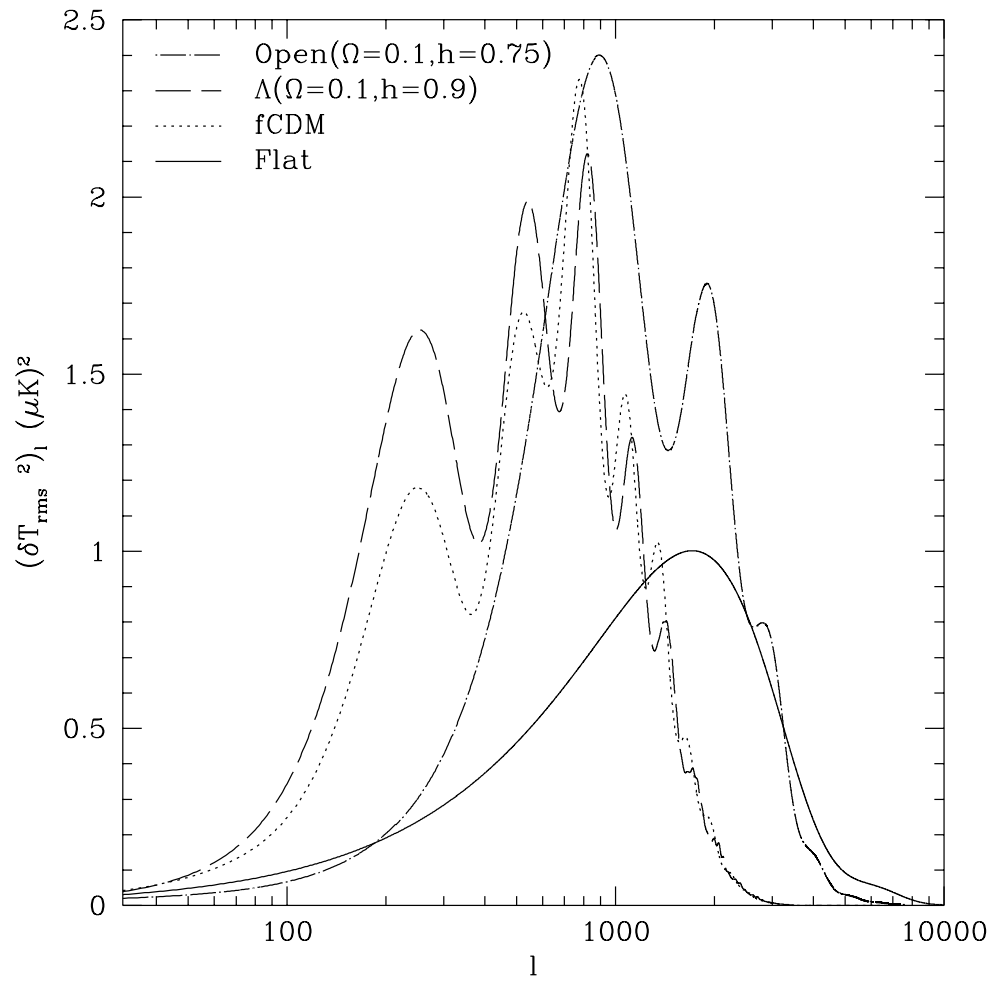


Figure 3

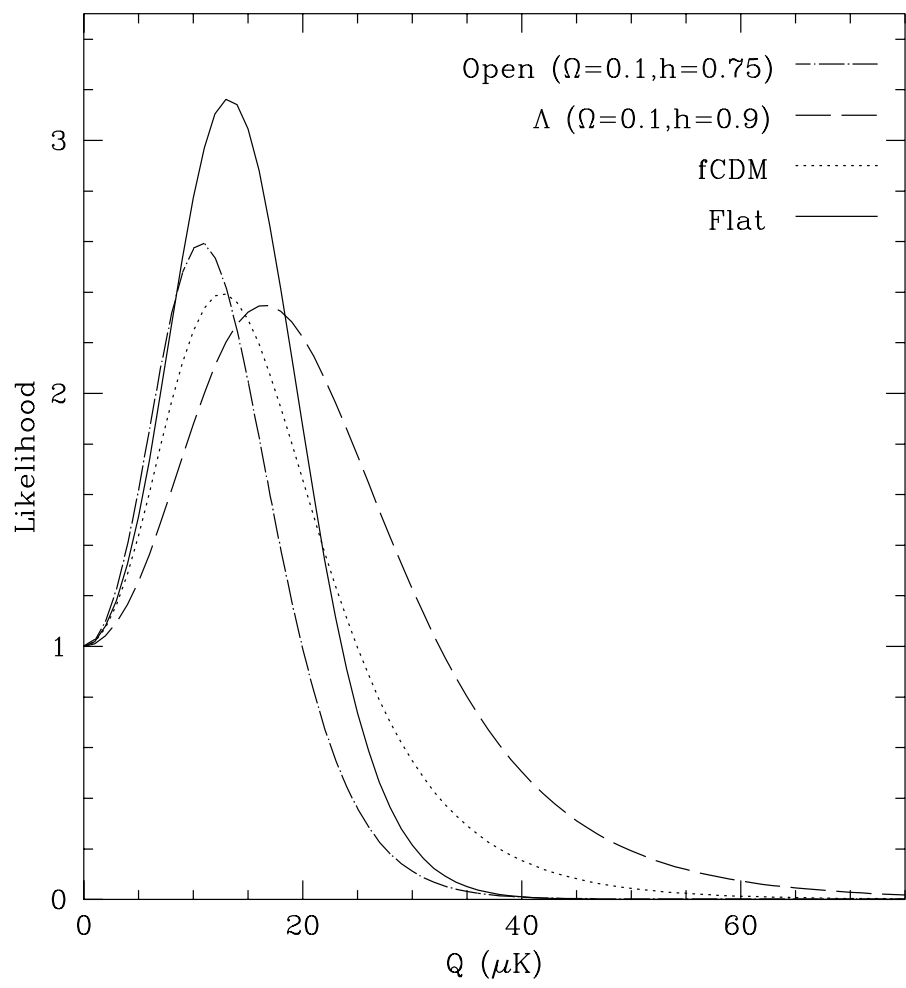


Figure 4